Int. J. Multiphase Flow Vol. 19, No. 6, pp. 1129–1151, 1993
Printed in Great Britain

0301-9322/93 $6.00 + 0.00
Pergamon Press Ltd

BIFURCATION PHENOMENA IN TWO-PHASE NATURAL CIRCULATION

A. KNAANI and Y. ZVIRIN
Faculty of Mechanical Engineering, Technion—Israel Institute of Technology, Haifa 32000, Israel

(Received 19 May 1990; in revised form 31 August 1993)

Abstract—Multiple steady-state solutions have been found theoretically for a two-phase natural circulation loop. This bifurcation phenomenon is attributed to the nonmonotonic behavior of the buoyancy and friction forces, and the discontinuities due to transitions between two-phase flow patterns. The paper outlines a general and consistent modeling method to describe two-phase natural circulation at steady state. The solution of the one-dimensional governing conservation equations is performed by a combination of analytical and numerical stages. The method is implicit, to treat the highly nonlinear problem by multinested iteration loops. Results are presented and discussed for the multiple solutions of the flow rate, temperature, quality and void distributions and two-phase elevations. Pressure effects are also studied. A comparison with available data shows that the theoretical model simulates the important characteristics of two-phase thermosyphons.

Key Words: two-phase natural circulation, two-phase thermosyphon, two-phase free convection loop, bifurcation, multiple steady-state solutions

1. INTRODUCTION

Natural circulation loops (thermosyphons) appear in geophysical and geothermal processes and have a wide range of applications in diverse energy conversion systems, like solar heating devices, magneto hydrodynamic generation of electricity and emergency core cooling of nuclear reactors. Several of these thermosyphons involve two-phase flows. The reviews of Zvirin (1981) and Greif (1988) summarize the theoretical and experimental investigations of the steady state, transient behavior and stability characteristics of natural circulation loops, with the focus on single-phase thermosyphons.

It is well-known that free convection loops exhibit some peculiar stability features. These have an obvious fundamental physical interest and important operational implications in energy conversion systems. Three different types of instabilities have been found, theoretically and experimentally, in thermosyphon systems (except for the possible appearance of Rayleigh–Benard closed cells), cf. Zvirin (1985):

(1) The onset of bulk flow around the loop.
(2) The instability of a steady loop flow, caused by oscillations growth.
(3) Multiple steady-state solutions, i.e. metastable equilibrium or bifurcation.

Beside these instabilities, it has been found that "chaotic" behavior sometimes exists (cf. Hart 1984). Bifurcation in single-phase thermosyphons has been discovered in systems with parallel branches (Chato 1963; Jeuck *et al.* 1981), in loops with throughflows, i.e. mixed convection (Mertol *et al.* 1981), and double-diffusive natural circulation (Rubenfeld & Siegmann 1977; Zvirin 1987, 1991). The processes in these loops are more complex than in "simple" ones, where the flow and heat transfer are governed by buoyancy and friction only.

It is noted that bifurcation phenomena occur in other flow systems, e.g. the well-known hydraulic jump in single-phase open-channel flow with a pressure head. Many two-phase flow systems exhibit multiple solutions, e.g. in a multitude of parallel channels, as reviewed by Hetsroni (1982). Multiple solutions are also associated with other flow phenomena, e.g. oscillations due to density waves. An important conclusion was derived by Sen & Treviño (1983) and Ramos *et al.* (1985), implying that multiple solutions can be obtained for two-phase thermosyphons by one-dimensional models for constant and variable areas.

Two-phase natural circulation phenomena occur in reboilers, frequently used in the chemical engineering industry. McKee (1970) surveyed the relevant literature and suggested flow and heat transfer correlations for design purposes. Early work on two-phase natural circulation relevant to nuclear reactors included experiments aimed at measuring parameters such as flow rates and heat transfer coefficients (Piret & Isbin 1954) and studying flow oscillations (Wissler *et al.* 1956). The application of thermosyphons in this field has attracted increased interest following the accidents in TMI and Chernobyl. Several experimental rigs were constructed and tested (e.g. Kiang & Marks 1981; Cundy & Ha 1982; Nguyen-Chi & Banerjee 1984), which provided data and information about various two-phase natural circulation processes, including transitions between flow regimes.

The need for practical safety criteria and simulation of transients such as small-break natural circulation, lead to the development of scaling laws to interpret results obtained from experimental models of various sizes and to predict from them the behavior of prototypical reactor systems. These derivations (e.g. Ishii & Kataoka 1983; Ishii *et al.* 1986; Kiang 1985; Zvirin & Sursock 1987) are based on dimensional analysis of the governing conservation equations, without actually solving them. The stability of flow systems with multiple parallel channels is governed by different dimensionless groups (cf. Bouré & Mikaila 1967; Ishii & Zuber 1970). Bouré & Mikaila (1967) presented a stability diagram which uses dimensionless velocity and enthalpy as parameters. Ishii & Zuber (1970) used subcooling and phase-change numbers for the construction of their stability chart. There does not yet exist a general consistent theoretical model to describe and simulate two-phase natural circulation loops. The few existing theoretical models, mostly one-dimensional, apply to specific loops, are limited by basic simplifying assumptions and do not take into account the various two-phase flow regimes and the transitions between them.

Reed & Tien (1987) studied theoretically and experimentally a thermosyphon enclosed in a cylinder, with evaporation at the bottom, an upwards loop flow inside an inner tube and condensation in the annulus around it. Ardron & Krishnan (1984) studied the stability of a certain loop, but their method is not accurate because they did not consider all the equations which govern the stability characteristics. Duffey & Sursock (1987) developed a theoretical method for calculating steady-state situations in two-phase thermosyphons. Although some of the assumptions in their method are quite simplified and most of the phenomenological parameters are based on average loop properties, the fundamental physical features are kept. Thus, they could show the important phenomenon of a local maximum for the flow rate when the input power is increased. This had been previously obtained in the experiments of Loomis & Soda (1982) and Shimeck & Johnsen (1984). One disadvantage of the model of Duffey & Sursock (1987) is that no attention is given to transitions between flow regimes and patterns.

As mentioned above, available information about bifurcation phenomena in two-phase natural circulation is quite scarce. Multiple steady-state solutions are not easy to detect, especially if some of them are unstable. The existing theoretical methods are not always capable of predicting such solutions, e.g. because they lack the details of transitions between flow regimes. As explained above, the mechanisms leading to bifurcation require triggering which extends beyond the balance of buoyancy and friction forces in a "simple" loop. Ramos *et al.* (1985) indicated that bifurcation exists in two-phase thermosyphons, but their theoretical model is an extension of that for single phase, assuming constant friction and heat transfer coefficients. Such assumptions are too simplified for the description of two-phase flow.

A more extensive literature survey appears in Knaani (1990). The objective of the present work, stemming from this survey, summarized above, is to develop a more general and consistent theoretical method to characterize two-phase natural circulation. The next section includes derivation of the mathematical model, based on integral momentum equation, and a flow regime map adopted from a drift-flux representation with appropriate correlations for friction, heat transfer and void-quality. Sections 3 and 4 describe the analytical–numerical solution procedure. Results are presented in section 5, for an example of a simple geometry loop, in order to demonstrate application of the method and to study several important and interesting phenomena, including bifurcation (multiple steady solutions), pressure effects and sensitivity to the choice of the flow regime map.

The analytical treatment of the governing differential equations leads to a set of nonlinear algebraic equations. It is noted that there is no guarantee, *a priori*, that a solution would always

exist for such equations, particularly because of the discontinuity of the correlations at the transition between flow regimes. For example, Grossman *et al.* (1987) developed a theoretical method to analyze cooling absorption cycles, and could not obtain a solution in the whole range of the parametric space. Here the results were obtained for a continuous wide range of system parameters; input power, pressure and geometry, and reconstruct trends which have been previously observed in experiments, i.e. local maxima of the flow rate curves as functions of the power and pressure.

2. THE THEORETICAL MODEL

The loop considered here, shown schematically in figure 1, consists of heated and cooled branches (heat source and sink) connected by short sections at the top and bottom. Knaani (1990) outlined a general consistent approach to describe natural circulation in more complex systems, relevant to the cooling loops of nuclear reactors, with hot and cold legs and arbitrary elevations of the source and sink. He derived the transient conservation equations governing the flow and heat transfer in such two-phase thermosyphons. The method is based, in part, in some previous treatments mentioned above (e.g. Ishii & Kataoka 1983; Ishii *et al.* 1986; Kiang 1985; Zvirin & Sursock 1987). Application of the method for the loop in figure 1 has been chosen in order to demonstrate its use and to study several important processes, phenomena and effects.

Two operational modes of the natural circulation system are studied: either with a pressurizer (or expansion tank), not shown in figure 1, or without it. In the first case the pressure is specified *a priori*, determining the fluid properties, including T_{sat}. In the second case, the total fluid mass (inventory) of the completely closed loop is given, and the pressure is obtained as part of the solution.

The governing equations are written in one-dimensional form for the steady state, where s is the coordinate running around the loop and Z is the vertical one. Thus, all the variables are averaged over the cross section. Other approximations are that the subcooled length can be neglected, there is no condensation in the riser and a drift-flux equilibrium approach is taken for the two-phase flow regimes. Incompressible flow is considered, and the Boussinesq approximation is adopted, whereby the fluid properties are taken as constant except for the density in the gravity term of the

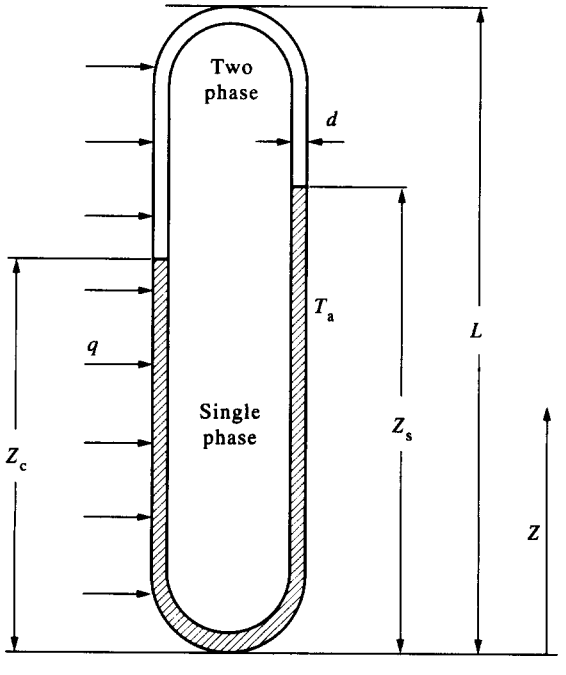

Figure 1. Schematic of the two-phase natural circulation loop.

momentum equation, where:

$$\rho = \rho_L[1 - \beta(T - T_{sat})] \qquad \text{single phase} \qquad [1a]$$

and

$$\rho = \rho_L[1 - (1 - \gamma)\epsilon] \qquad \text{two phase;} \qquad [1b]$$

$T(s)$ and $\epsilon(s)$ are the temperature and void fraction, β is the thermal expansion coefficient, γ is the density ratio, $\gamma \equiv \rho_G/\rho_L$ and T_a is a temperature of the secondary fluid (or ambient) of the sink, taken as constant.

The continuity equation yields the result that the mass flow rate in the loop is uniform, thus for steady state $\dot{m} = \text{const}$, *a priori* unknown. The momentum equation is written in a general form, for both the single- and two-phase regions:

$$\frac{\partial}{\partial s}\left(\frac{\dot{m}^2}{\rho A}\right) + \frac{\partial}{\partial s}\left[\frac{\epsilon\rho_L\rho_G}{(1-\epsilon)\rho} U_{Gu}^2\right] = -\frac{\partial p}{\partial s} - \rho g - \frac{1}{2}K'\frac{\dot{m}^2}{\rho A^2}, \qquad [2]$$

where $A = \pi d^2/4$. Except for the terms representing inertia, pressure, gravity and friction forces, the equation includes the term of the drift stress. It depends on the local drift-flux velocity, U_{Gu}, characterizing the imbalance of the velocities of the phases. For single-phase flows this term identically vanishes: $U_{Gu} = 0$ for pure vapor and $\epsilon = 0$ for pure liquid. K' in [2] is the local friction parameter. As customary in problems of natural circulation, the momentum equation, [2], is integrated around the loop to eliminate all the gradient terms. This gives

$$-gB - \dot{m}^2\frac{K}{2A^2\rho_L} = 0, \qquad [3]$$

where K is the overall friction parameter

$$K = \frac{f}{d}[(Z_c + Z_s) + \Phi^2(2L - Z_c - Z_s)]; \qquad [4]$$

f and Φ^2 are the single-phase friction coefficient and the two-phase multiplier. B is the buoyancy integral

$$B \equiv \oint \rho \, dZ = \rho_L\{[1 - \bar{\epsilon}_c(1-\gamma)](L - Z_c) - [1 - \bar{\epsilon}_s(1-\gamma)](L - Z_s) + Z_c[1 - \beta(\bar{T}_c - T_{sat})] - Z_s[1 - \beta(\bar{T}_s - T_{sat})]\}, \qquad [5]$$

where the mean temperatures and void fractions in the heat source and sink are defined by

$$\int_0^{Z_s}(T_s - T_{sat})\,dZ \equiv Z_s(\bar{T}_s - T_{sat}), \quad \int_0^{Z_c}(T_c - T_{sat})\,dZ \equiv Z_c(\bar{T}_c - T_{sat}) \qquad [6]$$

and

$$\int_{Z_s}^{L}\epsilon_s\,dZ \equiv (L - Z_s)\bar{\epsilon}_s, \quad \int_{Z_c}^{L}\epsilon_c\,dZ \equiv (L - Z_c)\bar{\epsilon}_c; \qquad [7]$$

L is the height of the loop and Z_s and Z_c are the two-phase elevations (see figure 1). The subscripts c and s denote the source and sink.

The energy equation is written separately for the single- and two-phase regions in the heated branch,

$$\dot{m}c_p\frac{dT}{dZ} = q \qquad 0 \leqslant Z \leqslant Z_c \qquad [8a]$$

and

$$\dot{m}H_{LG}\frac{dx}{dZ} = q \qquad Z_c \leqslant Z \leqslant L \qquad [8b]$$

and in the cooled channel,

$$\dot{m}c_p \frac{dT}{dZ} = h_{sp}\pi d(T - T_a) \qquad 0 \leqslant Z \leqslant Z_s \qquad [9a]$$

and

$$\dot{m}H_{LG} \frac{dx}{dZ} = h_{tp}\pi d(T_{sat} - T_a) \qquad Z_s \leqslant Z < L; \qquad [9b]$$

where x is the vapor quality, q is the power input per unit length, H_{LG} is the latent heat, h_{sp} and h_{tp} are the single- and two-phase heat transfer coefficients in the sink. The latter is for condensation in downwards flow. In general q may depend on Z; here it is taken as constant, $q = Q/L$, where Q is the total input power.

The boundary conditions are continuity of the temperature at the bottom and the quality at the top:

$$T_c = T_s \equiv T_0 \quad \text{at} \quad Z = 0 \qquad [10a]$$

and

$$x_c = x_s \equiv x_l \quad \text{at} \quad Z = L. \qquad [10b]$$

For cases where the whole loop is single phase the energy equations are [8a] and [9a], and the top boundary condition is continuity of the temperature also.

In order to complete the mathematical formulation, i.e. closure of the model, it is necessary to specify the parameters f, Φ^2, h_{sp} and h_{tp}, and to employ a relation between ϵ and x. It is noted that the method developed by Knaani (1990), outlined above, is general and can be applied with any model representing two-phase flow and heat transfer. Here the drift-flux approach has been used and phenomenological correlations for the parameters have been chosen as described below. These parameters depend, in general, on the (unknown) flow rate, the vapor quality, the void fraction and the flow regimes and two-phase flow patterns. The coefficients f, Φ^2, h_{sp} and h_{tp} are taken as independent of the axial coordinate, i.e. their values express means over the respective sections.

The friction coefficient, f, is taken from the Moody diagram and the two-phase multiplier, Φ^2, from Chisholm (1967). For the heat transfer parameters the internal convection coefficients are used, because it is assumed that the resistance is much smaller in the tube wall and the external surfaces, where strong secondary forced flow usually prevails. h_{sp} is taken from standard correlations for laminar and turbulent flows and h_{tp} for the condensation region from Collier (1972).

The relation between the void fraction and quality, needed in the drift-flux model used here, is written as in Hetsroni (1982):

$$\epsilon_c = \frac{x\rho_L}{C_0[x\rho_L + (1-x)\rho_G] + \dfrac{\rho_L \rho_G U_{Gu}}{\dot{m}}}. \qquad [11]$$

The drift-flux velocity, U_{Gu}, and the distribution parameter, C_0 are taken from Kaizerman *et al.* (1982). They depend on the two-phase flow patterns, thus a flow regimes map is needed, which is taken from Kaizerman *et al.* (1983). All the details and various expressions for the correlations appear in the appendices of Knaani (1990). The relation for $\epsilon(x)$, [11] is used for the heat source, in which boiling upwards flow occurs. No equivalent correlations have been found for the condensing downwards flow in the heat sink. Therefore, a linear relation between ϵ and x is assumed there. The sensitivity of the results to the transition limits in the two-phase flow regimes map is studied, as will be seen below. It is finally noted that there are other models to represent two-phase flow regimes and patterns, e.g. the drift-flux model of Chexal & Lellouche (1985/1986) and the more basic approach by Barnea (1987) of directly using the phase superficial velocities. In the first stages of this work some attempts have been made to employ other models, and the correlations and map of Kaizerman *et al.* (1982, 1983), as well as the other flow and heat transfer correlations, were then chosen because they proved to be more convenient for both the theoretical modeling and the numerical algorithm.

For generality of the solution procedure, the governing equations are transformed to dimensionless form. For this, scaling of the variables is defined by

$$z \equiv \frac{Z}{L}, \quad \theta = \frac{T - T_a}{\Delta T}, \quad \omega \equiv \frac{\dot{m}}{\dot{m}_{sp}}, \tag{12}$$

where

$$\Delta T \equiv T_{sat} - T_a, \quad \dot{m}_{sp} = \frac{Q}{c_p \Delta T}. \tag{13}$$

As in the other problems of natural convection, there is no characteristic velocity here. The reference flow rate, $\dot{m}_{sp}$, is chosen as that at the limiting case where the bottom temperature equals that of the ambient and the top one just reaches saturation.

Introduction of [12] and [13] into [4]–[11] yields the following formulation. The momentum equation is reduced to

$$F(\omega) = N_{bf} b - \omega^2 = 0, \tag{14}$$

where the dimensionless bouyancy integral is given by

$$b = (1-\gamma)[\bar{\epsilon}_c(1-z_c) - \bar{\epsilon}_s(1-z_s)] + \beta \Delta T[(\bar{\theta}_c - \bar{\theta}_s) + (z_s - z_c)] \tag{15}$$

and the mean values $\bar{\epsilon}$ and $\bar{\theta}$ are defined by

$$\bar{\epsilon}_i \equiv \frac{1}{1-z_i}\int_{z_i}^{1} \epsilon_i \, dz, \quad \bar{\theta}_i \equiv \frac{1}{z_i}\int_{0}^{z_i} \theta_i \, dz; \qquad i = c, s. \tag{16}$$

The energy equations for the heat source are transformed to

$$\frac{d\theta}{dz} = \frac{1}{\omega} \qquad 0 \leqslant z \leqslant z_c \tag{17a}$$

and

$$\frac{dx}{dz} = \frac{St}{\omega} \qquad z_c \leqslant z \leqslant 1; \tag{17b}$$

and those for the sink to

$$\frac{d\theta}{dz} = \frac{N_{ssp}}{\omega}\theta \qquad 0 \leqslant z \leqslant z_s \tag{18a}$$

and

$$\frac{dx}{dz} = \frac{N_{stp}}{\omega} \qquad z_s \leqslant z \leqslant 1. \tag{18b}$$

The dimensionless groups which appear in these equations are defined by

$$N_{bf} \equiv \frac{2g\rho_L^2 LA^2}{K\dot{m}_{sp}^2}, \quad St \equiv \frac{c_p \Delta T}{H_{LG}}, \quad N_{ssp} \equiv \frac{h_{sp}\pi dL}{c_p \dot{m}_{sp}}, \quad N_{stp} \equiv \frac{h_{tp}\pi dL \Delta T}{H_{LG}\dot{m}_{sp}}. \tag{19}$$

The dimensionless form of the boundary conditions is

$$\theta_c = \theta_s \equiv \theta_0 \quad \text{at } z = 0 \tag{20a}$$

and

$$x_c = x_s \equiv x_1 \quad \text{at } z = 1. \tag{20b}$$

Finally, the relation for $\epsilon_c(x)$, [11], reduces to

$$\epsilon_c = \frac{x_c}{C_0[x_c + (1-x_c)\gamma] + \dfrac{\gamma u_{Gu}}{\omega}}, \tag{21}$$

where $u_{Gu} \equiv \rho_L A U_{Gu}/\dot{m}_{sp}$.

3. THE STEADY-STATE SOLUTION

The solution procedure for the above set of simultaneous integro-differential equations consists of a combination of analytical and numerical stages. The flow charts in figures 2a–c summarize the algorithm described below and the numerical procedure outlined in section 4. First, the energy equations are solved in terms of the unknown constant, ω. The solution of [17a, b] for the heat source yields the linear distributions of the temperature and quality:

$$\theta_c = \theta_0 + \frac{z}{\omega} \quad 0 \leqslant z \leqslant z_c \qquad [22a]$$

and

$$x_c = \frac{\mathrm{St}}{\omega}(z - z_c) \quad z_c \leqslant z \leqslant 1. \qquad [22b]$$

The dimensionless bottom temperature, θ_0, is also unknown. The source two-phase elevation, z_c, is that where the temperature reaches saturation:

$$z_c = \omega(1 - \theta_0). \qquad [23]$$

It is assumed that the subcooled boiling region is negligible. For the heat sink the solution of the energy equations [18a, b] is

$$\theta_s = \theta_0 \exp\left[\frac{N_{ssp} z}{\omega}\right] \quad 0 \leqslant z \leqslant z_s \qquad [24a]$$

and

$$x_s = \frac{N_{stp}}{\omega}(z - z_s) \qquad z_s \leqslant z \leqslant 1, \qquad [24b]$$

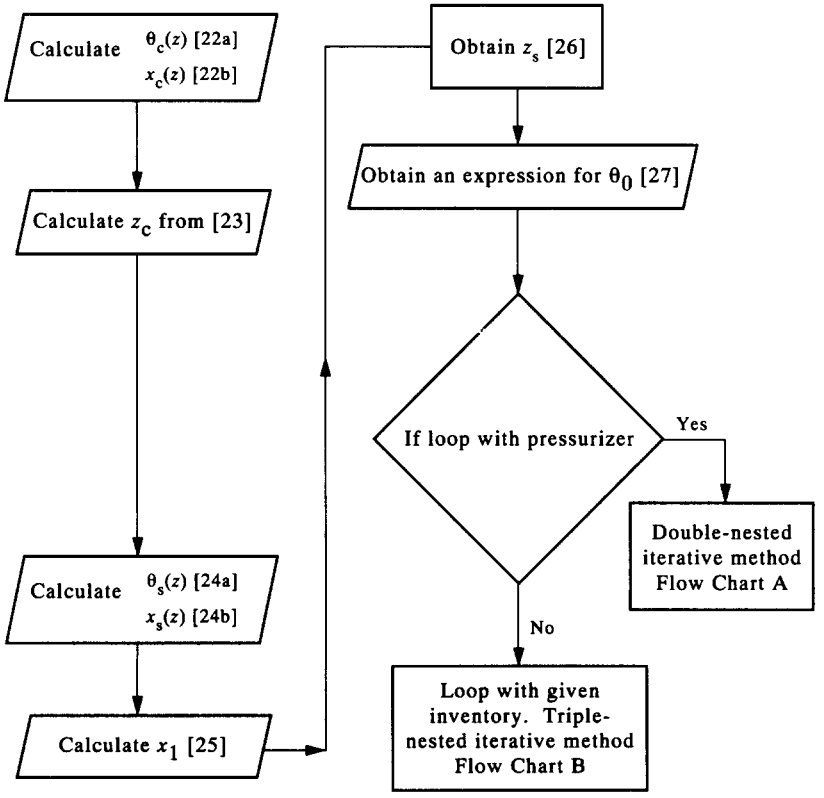

Figure 2a. Flow chart of the solution algorithm.

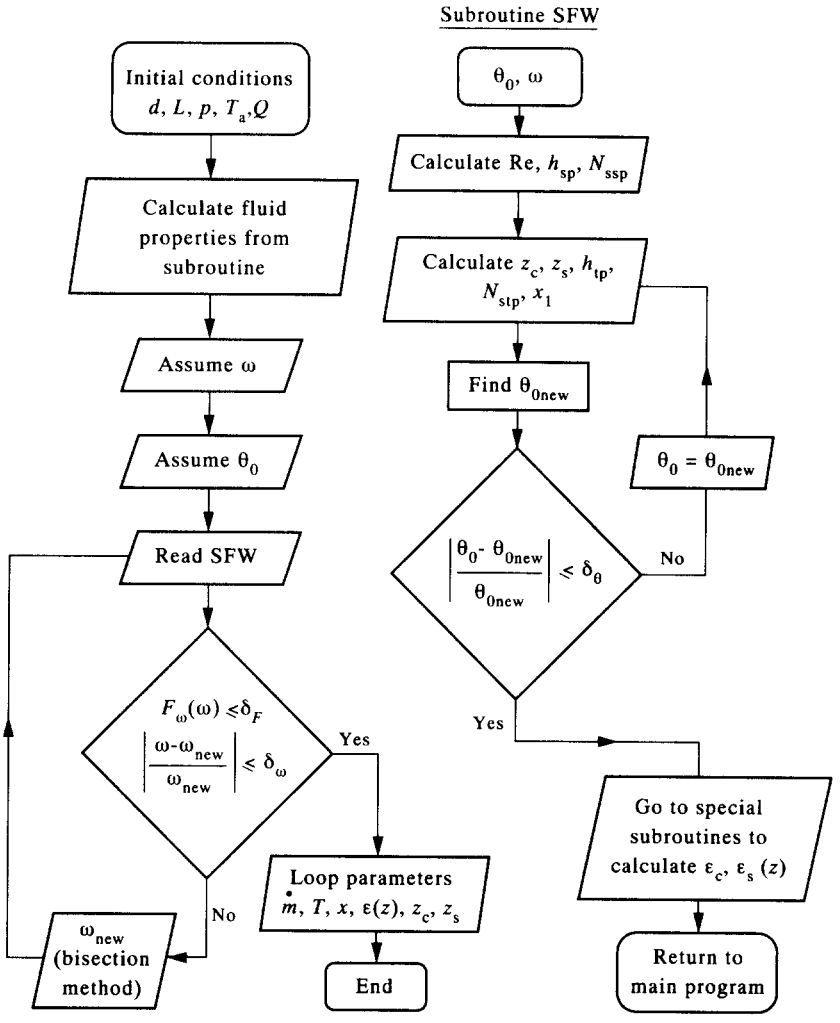

Figure 2b. Flow chart (A) of the numerical procedure for a loop with a pressurizer.

where use has been made of the condition that the flow returns to single phase, $x_s = 0$, at the elevation z_s. The boundary condition [20b] of continuity of the vapor quality at the top is applied now to eliminate x_1 from [22b] and [24b]:

$$x_1 = \frac{\mathrm{St}}{\omega}(1 - z_c) = \frac{N_{stp}}{\omega}(1 - z_s) \quad \text{at } z = 1. \tag{25}$$

This leads to the following relationship between the two-phase elevations:

$$z_s = 1 - \frac{\mathrm{St}}{N_{stp}}(1 - z_c). \tag{26}$$

As mentioned above, the bottom temperature is not known. In order to find it, the saturation condition, $\theta_s = 1$ at $z = z_s$, is employed. Then using [24a], [26] and [19], the following expression is obtained:

$$\theta_0 = \exp\left(-\frac{N_{ssp}}{\omega} z_s\right) = \exp\left[\frac{h_{sp}(1-\omega)}{h_{tp}\omega}\right] \exp\left(-\frac{N_{ssp}}{\omega}\right) \exp\left(\frac{h_{sp}}{h_{tp}} \theta_0\right). \tag{27}$$

This is an implicit equation for θ_0 in terms of ω, which, in general, has to be solved numerically, by an iterative method, after solving the energy equations (as explained below), because h_{tp} depends on x_1. Since both ω and θ_0 are unknown, the general iterative solution procedure is at least double-nested. However, for very low top qualities, Collier's (1972) expression for h_{tp} yields a value which is lower than h_{sp}. Since this is not realistic, it is assumed that $h_{tp} = h_{sp}$ in this narrow range

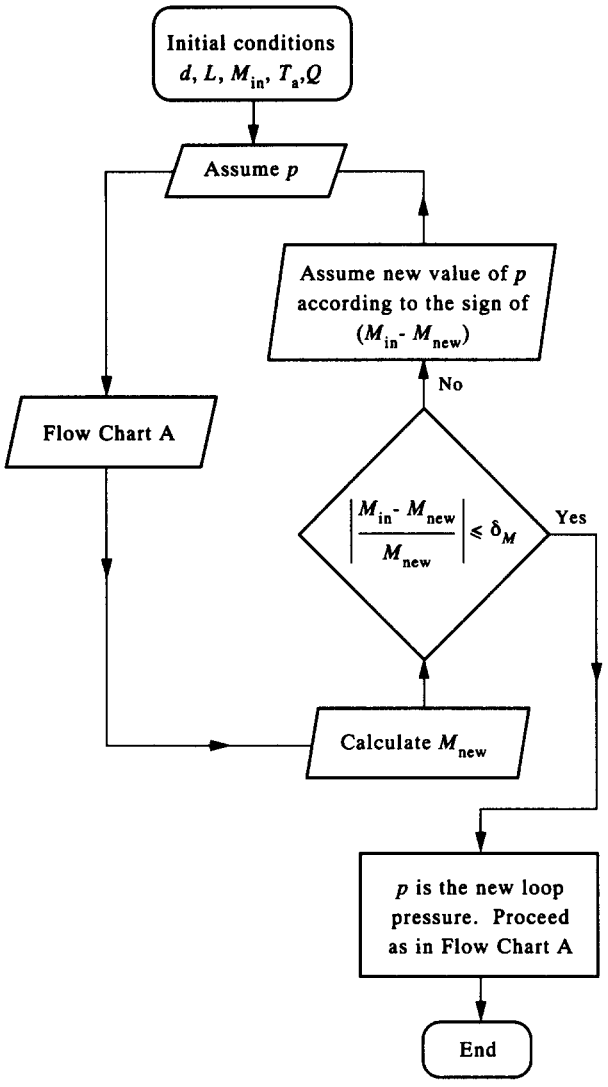

Figure 2c. Flow chart (B) of a loop with a given inventory.

and [27] yields a direct numerical solution for θ_0. This feature is important and convenient in the first stages of the complete numerical solution of the whole loop. For higher Q, an appropriate first guess for θ_0 can be chosen as the known solution for a somewhat lower power.

Once the temperature and vapor quality are known, the buoyancy integral [15] can be computed and introduced into the momentum equation [14] to yield an implicit algebraic equation for the dimensionless mass flow rate, ω. For this the void fraction distribution is needed. ϵ_s in the sink was assumed to depend linearly on x_s, which is a linear function of z, cf. [24b]. Therefore,

$$\epsilon_s = \frac{\epsilon_1(z - z_s)}{(1 - z_s)} \qquad [28]$$

where ϵ_1 is the top void fraction, $\epsilon_1 = \epsilon_c(z = 1)$. For the source, $\epsilon_c[x_c(z)]$ is calculated by [21]. It is noted that since the parameters C_0 and u_{Gu} depend, in general, on ϵ_c, this is an implicit equation for ϵ_c. Hence, the numerical solution involves a triple-nested iterative procedure, or quadruple for the case of unknown pressure. The numerical method is described in the next section, which also includes the final stages of derivation of the buoyancy integral.

The particular case of a single phase is easier to solve. Here the top boundary condition [20b]

is replaced by continuity of the temperature at $z = 1$, and instead of [27] for θ_0 we get

$$\theta_{0sp} = \frac{1}{\omega\left[\exp\left(\frac{N_{ssp}}{\omega}\right) - 1\right]}. \quad [29]$$

The buoyancy integral [15] is calculated by introducing the distributions [22a] and [24a]:

$$b_{sp} = \frac{\beta\Delta T}{\omega}\left[0{\cdot}5 - \frac{\omega}{N_{ssp}} + \frac{1}{\exp\left(\frac{N_{ssp}}{\omega}\right) - 1}\right]. \quad [30]$$

This relation is finally inserted in the momentum equation [14], where the parameter N_{bf} includes the single-phase friction parameter $K_{sp} = 2fL/d$. The resulting equation,

$$\omega = \sqrt{N_{bf} b_{sp}}, \quad [31]$$

is solved numerically, because both b_{sp} and K_{sp} depend on ω. The successive approximations or Newton–Raphson method has been used to solve it. Single-phase results are not shown in the present paper. Knaani (1990) and Knaani & Zvirin (1990) include some results for the lower range of the input power.

4. NUMERICAL SOLUTION PROCEDURE

Let us consider, first, the case of a loop with a pressurizer, where the pressure is specified and determines the saturation temperature, T_{sat}. The saturation properties such as ρ_L, ρ_G and H_{LG} are also determined, and those for the single phases, e.g. viscosity, thermal conductivity and specific heat, are taken at T_{sat}. The algebraic (momentum) equation [14] is solved to obtain the dimensionless mass flow rate, ω. Then the other loop variables are found: the temperature, quality and void distributions and the two-phase elevations, z_c and z_s.

A computer program was developed for the numerical solution. The program is quite general: all the calculations requiring specific models, e.g. the flow regimes map and the phenomenological correlations, are performed in subroutines, called by the main program. Parts of the solutions obtained analytically, such as the temperature and void fraction distributions and their integrals (for the buoyancy term), are also carried out in special subroutines. The program reads the input parameters: geometrical (d and L here) and operational (p, Q, T_a) data. The fluid properties (see above) are calculated from tables and interpolations in a subroutine. Then the parameters which depend only on these properties and the input data are computed ($\dot{m}_{sp}$, St). Initial values are chosen as "first guesses" for the dimensionless flow rate, ω, and bottom temperature, θ_0. The outer interaction loop is begun with this ω; the Reynolds number and then h_{sp} are calculated and N_{ssp} is obtained by [19]. The inner iteration loop to find θ_0 commences by solving [27] iteratively, by the successive approximations method. It is noted that its convergence is guaranteed because the absolute value of the derivative of the function of θ_0 on the RHS is < 1 in the whole solution range. The loop consists of the following stages, starting from an initial value of θ_0: z_c is calculated from [23], then x_1 from [25]. The two-phase heat transfer coefficient, h_{tp} is computed (from the appropriate correlation, in a special subroutine), then [19] is used to find N_{stp} and z_s is obtained from [25]. Finally, a new value for θ_0 is calculated by [27] and the internal loop is repeated until convergence is achieved, for the "current" value of ω in the outer loop. As explained above, for low Q when evaporation is just beginning (at the very top), $h_{tp} = h_{sp}$ and [27] is solved directly. Then an initial guess for $\theta_0(\omega)$ for a certain power is chosen as the solution for the previous, lower, Q.

Now the parameters in the momentum equation [14] are calculated. The means $\bar{\theta}_c$, $\bar{\theta}_s$, $\bar{\varepsilon}_c$ and $\bar{\varepsilon}_s$, needed for the buoyancy integral, b, are evaluated. The temperature profiles [22a] and [24a] are introduced with θ_0 into the integrals [16] for $\bar{\theta}_c$ and $\bar{\theta}_s$, which are obtained analytically:

$$\bar{\theta}_c = z_c\left(\theta_0 + \frac{z_c}{2\omega}\right) \quad [32]$$

and

$$\bar{\theta}_s = \frac{\theta_0 \omega}{N_{ssp}} \left[\exp\left(\frac{N_{ssp} z_s}{\omega} - 1 \right) \right]. \quad [33]$$

The mean void fractions $\bar{\epsilon}_c$ and $\bar{\epsilon}_s$ in [16] are calculated in subroutines, using [21], the solutions [22b] and [24b] for the qualities and the correlations for U_{Gu} and C_0. These depend on the two-phase flow patterns, determined by the local void fraction, ϵ, and the mixture velocity, V_m. Therefore, in the subroutine for the heat source the flow regime is checked at every point z according to the map, then U_{Gu} and C_0 are computed or determined. The reader is reminded that for some of the flow regimes the correlations depend on ϵ, thus an iterative numerical solution is performed to find the void fraction. $\bar{\epsilon}_c$ is found by Simpson's quadrature, after ϵ_c is computed at N points, equally spaced, in the evaporation portion of the heat source, $z_c \leqslant z \leqslant 1$.

In the subroutine for the sink, the integral for $\bar{\epsilon}_s$ is calculated analytically, from [28]:

$$\bar{\epsilon}_s = \epsilon_1 \frac{(1 - z_s)}{2}, \quad [34]$$

where the top void fraction, ϵ_1, has just been found. It is noted, again, that in the example considered here several stages of the solutions (of the differential equations and integrations) were done analytically. In other cases, for more practical systems, these would be performed numerically in the subroutines.

The means $\bar{\theta}_c$, $\bar{\theta}_s$, $\bar{\epsilon}_c$ and $\bar{\epsilon}_s$, which depend on ω, are introduced in [15] to calculate the buoyancy integral, b. The friction parameter, K, is calculated from [4], by using the correlations for f and Φ^2; both depend on ω, and the latter, using Chisholm (1967), on the mean vapor quality of the two-phase region of the loop. Since the profiles $x(z)$ are linear, [22b] and [24b], $\bar{x} = x_1/2$. Finally, N_{bf} is obtained from [19] and the value of the function $F(\omega)$ is computed from [14], in order to find the root of this equation. The outer iteration loop is repeated until [14] is satisfied within the required accuracy. Then all the converged final values are used, towards the end of the program, to evaluate all the output variables: mass flow rate, temperature, quality and void distributions and the two-phase elevations. The total loop mass (inventory), is also calculated:

$$M = M_{sp} + M_{tp} = \rho_L AL(z_c + z_s) + \rho_L AL\{(2 - z_c - z_s) - (1 - \gamma)[(1 - z_c)\bar{\epsilon}_c + (1 - z_s)\bar{\epsilon}_s]\}. \quad [35]$$

For the case of a completely closed system (without a pressurizer), with given inventory M_{in}, an additional iteration loop is performed: a value for the pressure is chosen as a first guess, then all the computations described above are performed. The value of M, obtained from [35], is compared with M_{in} and this outermost iteration is repeated until convergence is reached.

It is noted that [3] is the momentum equation integrated around the whole loop, to eliminate the pressure gradient term. Thus, [3] represents a balance of the overall buoyancy driving force and the retarding friction force. The pressure distribution can be obtained by integration of [2], after completion of the solution for $\dot{m}$, ρ, ϵ etc. Obviously, p increases and decreases in parts of the loop, to complete a cycle. K is then a friction parameter rather than a pressure loss coefficient. Within the approximation of the present work and taking into account the uncertainties, an average value for Φ^2 in the whole two-phase region was taken (depending on $\bar{x}$).

As mentioned above, the numerical solution requires double- or triple-nested iteration loops. It provides the dimensionless flow rate, ω, solving [14] which includes the function $F(\omega)$. The bisection method is employed to solve [14], because $F(\omega)$ has a very steep slope in some range of the system parameters, and other methods, i.e. secant, successive approximations, either would not converge or would be quite inefficient. One of the components of $F(\omega)$ is the dimensionless buoyancy integral, b [15]. This integral, which contains the terms, $\bar{\epsilon}_s$, $\bar{\theta}_s$ and $\bar{\theta}_c$, is computed numerically by the Simpson quadrature for N points of the heat source.

Table 1 shows the sensitivity of the solution (loop-dependent variables) to N and to the convergence criterion, δ_ω (see the flow chart in figure 2b), for a specific case and fixed values of the other convergence criteria, δ_θ and δ_F. As can be seen, these criteria are quite severe, in order to overcome the problems resulting from the behavior of $F(\omega)$ mentioned above, especially in the regions of bifurcation and transitions between flow regimes. Fortunately, however, these severe-

Table 1. Sensitivity of the numerical solution for the loop-dependent variables to: (a) the grid size of the heat source (number of divisions, N); (b) the convergence criterion δ_ω

	$F(\omega)$	ω	ϵ_1	z_c	z_s	x_1	θ_0
N							
10	−0.0002	0.9049	0.9763	0.1385	0.3758	0.1238	0.7371
50	0.0000	0.9333	0.9753	0.1421	0.3761	0.1195	0.7037
100	0.0001	0.9307	0.9754	0.1418	0.3760	0.1199	0.7057
δ_ω							
10^{-2}	0.0581	0.9350	0.9752	0.1424	0.3761	0.1193	0.7036
10^{-3}	−0.0052	0.9331	0.9753	0.1421	0.3761	0.1196	0.7037
10^{-4}	0.0000	0.9333	0.9753	0.1421	0.3761	0.1195	0.7037

$d = 0.02$ m, $p = 1$ bar, $Q = 24$ kW. Convergence criteria (see figure 2b): $\delta_\omega = 10^{-4}$, $\delta_\theta = 10^{-5}$, $\delta_F = 10^{-3}$; $N = 50$ (except when changed).

measures lead to high accuracy when convergence is reached. This is demonstrated in figure 3, showing convergence of $F(\omega)$ when N is increased: only very slight differences can be observed between the results for $N = 50$ and 100.

Knaani (1990) gives more details about the numerical analysis, the convergence patterns and the effects of the choice of grid points in the source and of the convergence criteria for the iterations loops on the results. As shown above, the solution is very sensitive to these parameters, which is reflected, for example, in the steepness of $F(\omega)$. Therefore, care must be taken, especially in the range of bifurcation, as discussed in the next section.

5. RESULTS AND DISCUSSION

The theoretical method developed in this work for describing the steady state in two-phase natural circulation was applied to the simple geometry loop (figure 1), in order to demonstrate its use and to investigate several phenomena and effects. Knaani & Zvirin (1990) studied the loop behavior for various values of the diameter and the input power, mostly at atmospheric pressure, without dwelling on the bifurcation phenomenon. In the present paper the main focus is on this feature, i.e. the existence of multiple steady-state solutions. The effect of the pressure on the loop characteristics is also studied. Additional results are included in Knaani (1990).

In the following we shall present the variables obtained from the numerical solutions as functions of the input power, Q, and the pressure, p for a loop with height $L = 1$ m, with diameter in the range $d = 0.02$ to 0.05 m (see figure 1) and secondary temperature $T_a = 30°C$. The output data

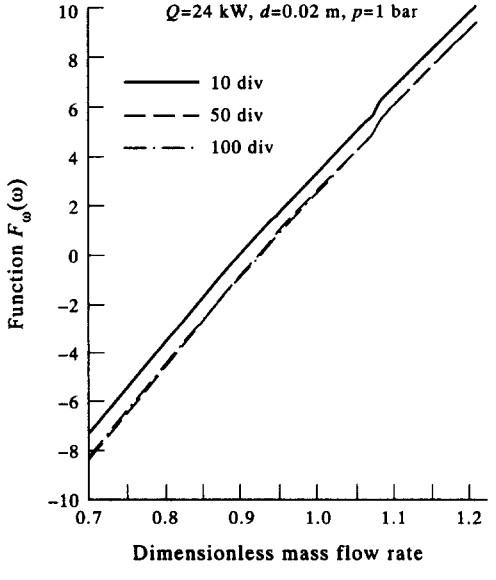

Figure 3. Sensitivity of the function $F(\omega)$ to the grid size of the heat source (number of divisions, N).

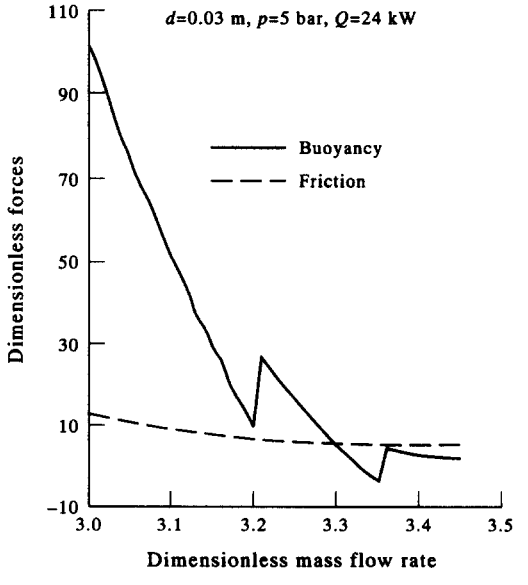

Figure 4. Dimensionless forces vs dimensionless mass flow rate.

include the mass flow rate, $\dot{m}$, the top void fraction and vapor quality, ϵ_1 and x_1 (at $z = 1$), the dimensionless two-phase elevations in the heat source and sink, z_c and z_s, and the bottom temperature, T_0 (at $z = 0$). In all cases (unless otherwise stated), the loop pressure is a known constant. The behavior of p for a closed system without a pressurizer and with given inventory is also discussed. The reader is reminded that use has been made of the two-phase flow regimes map of Kaizerman *et al.* (1983), with $\epsilon_{bs} = 0{\cdot}25$ and $\epsilon_{sa} = 0{\cdot}65$ for the transitions between bubbly and slug flow and between slug and annular flow. The sensitivity of the results to the selection of these values is also investigated.

5.1. Bifurcation—multiple steady-state solutions

The steady flow in the loop is governed by [14], which expresses the balance of the buoyancy driving force and the retarding friction force. Both depend on the flow rate and on the void and quality distributions and through them on the flow regime. The transitions between the various regimes are associated with discontinuities of the flow properties, in particular the void fraction and quality, which strongly affect the buoyancy and friction forces. These are plotted in figures 4 and 5 as functions of the flow rate for two examples with fixed d, p, and Q. It is noted that such graphs illustrate the behavior of the forces for given loop flows, as if at forced circulation; the difference between them would then be the required pumping head. The latter is identically zero at natural circulation, when the buoyancy and friction forces are equal, i.e., when their curves intersect at points representing the steady-state solutions. A single crossing of the lines means a single solution. As shown below, there is a range where bifurcation occurs, i.e. double or triple solutions when the lines intersect two or three times due to the nonmonotonous behavior of the buoyancy force. As mentioned in the introduction, bifurcation phenomena, emerging from similar force dynamics, appear in other two-phase flow systems and also in single-phase thermosyphons. Finally, it is noted that if the driving force, dominated here by the input power, is too low, it cannot overcome the friction, the force lines do not cross and there is no steady flow solution. Since the power is low, this situation is expected to occur in the single-phase (liquid only) range of the loop. Zvirin (1985, 1986) obtained critical Rayleigh numbers for the onset of flow in some natural circulation loops.

For the case shown in figure 4 there is a single crossing of the forces lines, indicating one root of [14] and a single steady-state solution. As can be seen, slight changes in the values of one or the two forces (for different input parameters) would lead to additional solutions, i.e. bifurcation or metastable equilibrium. Figure 5 describes, indeed, a situation where three different steady-state

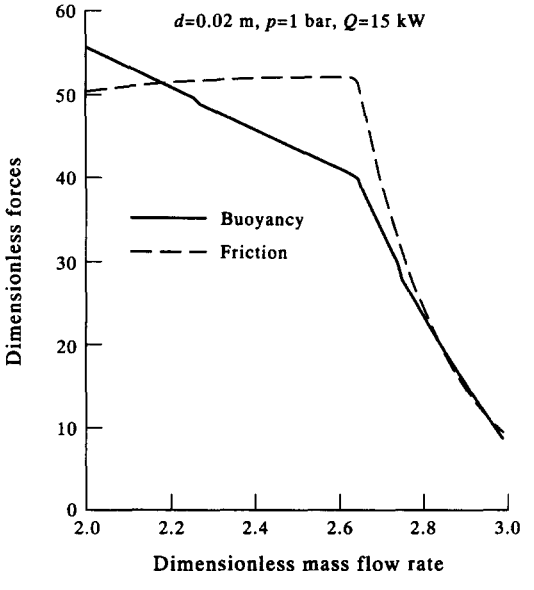

Figure 5. Dimensionless forces vs dimensionless mass flow rate.

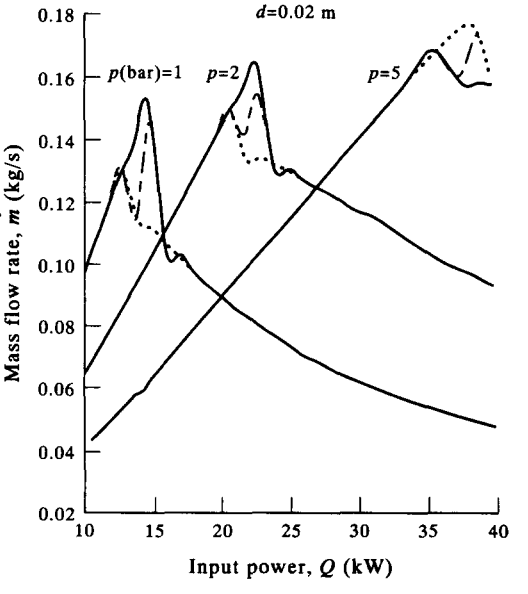

Figure 6. Multiple solutions for the mass flow rate, various pressures.

solutions exist. The point where the slopes of the curves change drastically corresponds to a transition between slug and annular flow, with sharp changes of ϵ and x. The general trend of the forces is to decrease when $\dot{m}$ increases, because then both ϵ and x diminish, reducing density changes on the one hand and the two-phase friction multiplier, Φ^2 (which strongly depends on x), on the other. Locally, slight opposite trends may occur, as seen for the friction force in figure 5, because it also depends on $\dot{m}^2$, and its effect counterbalances that of decreasing Φ^2.

It is noted that the present method describes steady-state flows in the loop. It is incapable of predicting the stability of the solutions; for this, either transient simulations of time-dependent problems or stability analyses are needed. In cases of multiple solutions in thermosyphons, all, some or none of them may be unstable (cf. Mertol *et al.* 1981).

The behavior of the mass flow rate, $\dot{m}$. as a function of the power input, Q, is described in figure 6 for several pressures, in the range where multiple solutions exist. As observed by Knaani & Zvirin (1990), there is a local maximum in the curves $\dot{m}(Q)$. This phenomenon, which was previously found theoretically by Duffey & Sursock (1987) and experimentally by Loomis & Soda (1982) and Shimeck & Johnsen (1984) and Serre *et al.* (1990), is explained by the behavior of the buoyancy and friction forces and the two-phase elevations, z_c and z_s. As Q is increased in the two-phase domain (after evaporation starts), both z_c and z_s start to decrease, with an increasing difference between them (as will be seen below), which enlarges the density variations and enhances the driving buoyance force, causing a rise in $\dot{m}$. On the other hand, the friction force also increases with Q due to the strong dependence of Φ^2 on the quality, and the decline of the circulating inventory, when the loop voids, thus $\dot{m}$ starts to decrease. Duffey & Sursock (1987) offer a somewhat different interpretation of the phenomenon, based on the behavior of the static pressure differential. The maximum of $\dot{m}$ shifts to higher Q when d and p rise (figure 6), as expected. When these increase beyond certain limits, the whole loop becomes vapor in single phase, before the maximum is reached. Additional results for $\dot{m}$, for wider ranges of d, p and Q and including liquid single phase at low Q, appear in Knaani & Zvirin (1990) and Knaani (1990).

As seen in figure 6, there is a rather narrow range where two or three solutions exist. The differences between them (for identical input parameters) become smaller with increasing pressure, mainly because of the smaller density changes. As explained above, the bifurcation is associated with the transitions between two-phase flow regimes, which also explains the oscillatory patterns of the curves $\dot{m}(Q)$ for all multiple solutions. It is noted that this bifurcation phenomenon was discovered only in regions where the transitions were found to occur. Moreover, a very careful treatment of the numerical solution (by increasing the accuracy) showed, indeed, convergence in all cases. It was found that by inserting the values obtained from the two or three different solutions into the governing equations, these are exactly satisfied. Thus, the multiple solutions are not due to numerical effects, but result from physical flow instabilities. The fact that the constitutive correlations are not continuous at the points chosen to represent transitions between flow regimes indicates that in reality these transitions are exhibited over some ranges, rather than at precise and exact limits or boundaries. The transitions fluctuate in these regions, depending on the configuration of the flow. Various disturbances can trigger the instabilities, causing switches from one flow regime to another, with different values of $\dot{m}$ and of the dependent variables. An observer might therefore see changes in the flow patterns and measure different values of the parameters associated with them. Finally, as mentioned above, thermosyphons and other flow systems exhibit various types of bifurcation phenomena.

Figure 7 illustrates the top void fraction and vapor quality, ϵ_1 and x_1 (at $z = 1$), for $d = 0.02$ m and $p = 1$ bar in the range of Q where multiple steady solutions exist. The types of the three lines are identical with those of figure 6, showing that the higher flow rate corresponds to lower void and quality, as expected. The latter starts growing sharply in the bifurcation range; this leads to a strong rise in the two phase multiplier, Φ^2, as explained above, which is the main reason for the subsequent drop in $\dot{m}(Q)$. In the whole range included in figure 7, the flow is annular at the top portion of the loop ($\epsilon > \epsilon_{sa} = 0.65$). For lower values of the input power, ϵ_1 and x_1 exhibits jumps at certain critical values of Q (depending on p and d), when transitions from bubbly to slug flow and slug to annular flow take place (cf. Knaani & Zvirin 1990). For higher pressures, the annular pattern is obviously established at higher powers.

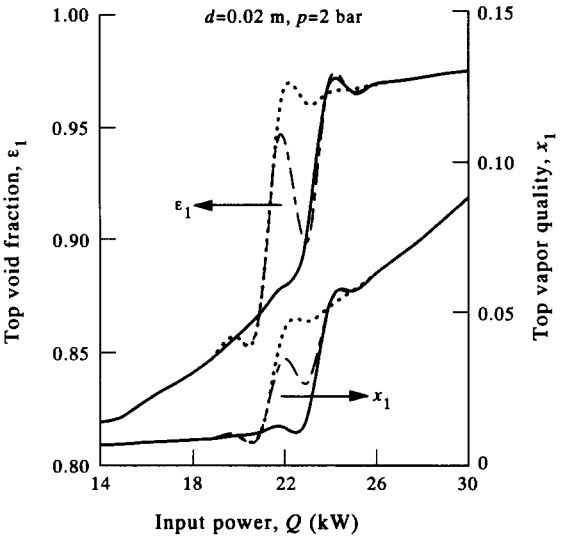

Figure 7. Multiple solutions for the top void fraction and vapor quality (line types correspond to those of figure 6).

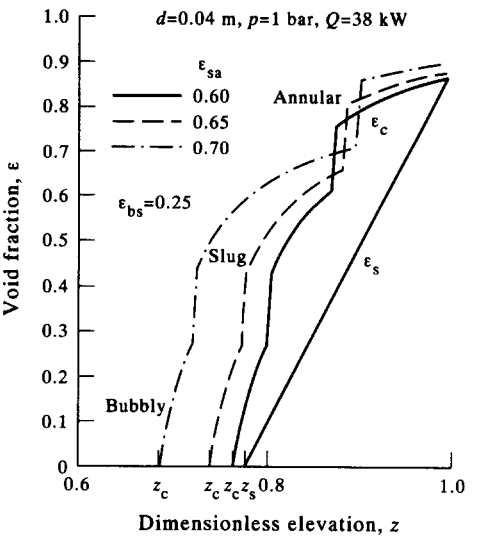

Figure 8. Void fraction distribution; sensitivity to the choice of the flow regimes map.

The void fraction distributions in the heat source ($z_c \leqslant z \leqslant 1$) and sink ($z_s \leqslant z \leqslant 1$) for a loop with $d = 0.04$ m, $p = 1$ bar and $Q = 38$ kW, are described in figure 8, which also shows the sensitivity of the results to the selection of the flow regimes map, discussed below. In the example considered here, the two-phase flow in the riser commences in a bubbly pattern, then switches to slug flow and later to the annular regime, with discontinuities at the transitions. In the downcomer, where the vapor condenses, a linear profile of $\epsilon(z)$ was assumed, as explained in section 2. This line is traced only once in the figure.

Figure 9 shows the multiple solutions for the two-phase elevations in the heat source and sink, z_c and z_s. Both decrease monotonically at low powers, then sharply in the neighborhood of the maximum flow rate. z_s is always larger than z_c, indicating a shorter condensing length in the downcomer than evaporation in the riser. This is due to the higher heat transfer coefficient, h_{tp}, in the former. h_{tp} increases with the quality, therefore at higher powers z_s decreases more moderately than z_c. Figure 10 describes the bottom temperature, T_0, for the same loop parameters as above.

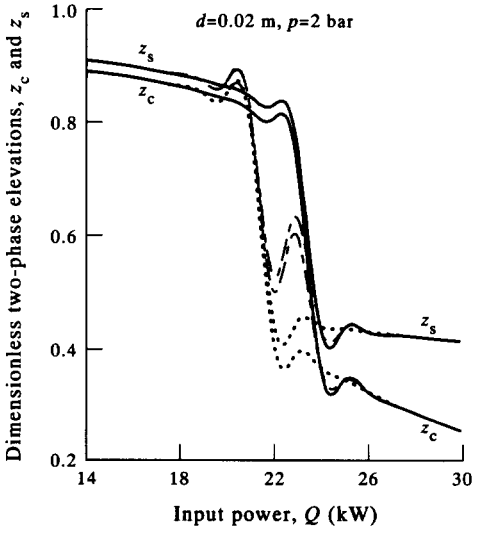

Figure 9. Multiple solutions for dimensionless two-phase elevations (line types correspond to those in figure 6).

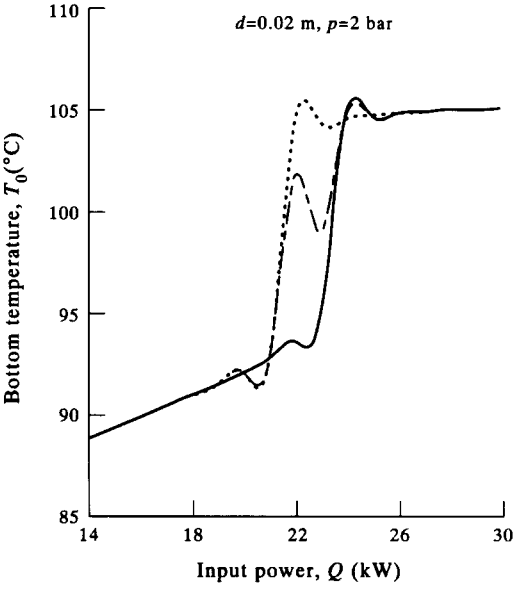

Figure 10. Multiple solutions for bottom temperature (line types correspond to those in figure 6).

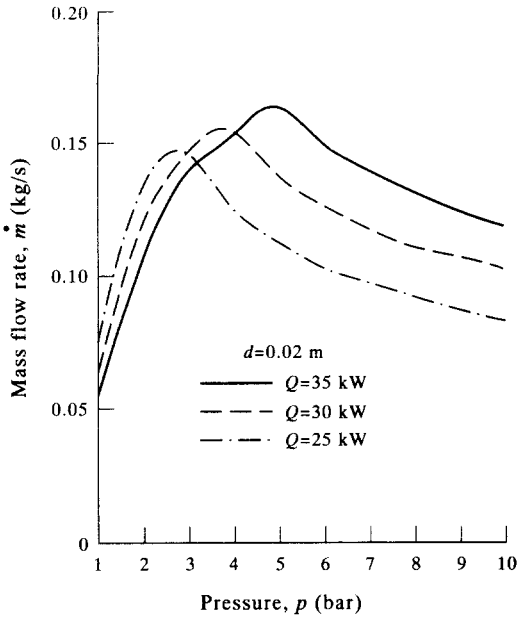

Figure 11. Mass flow rate vs loop pressure.

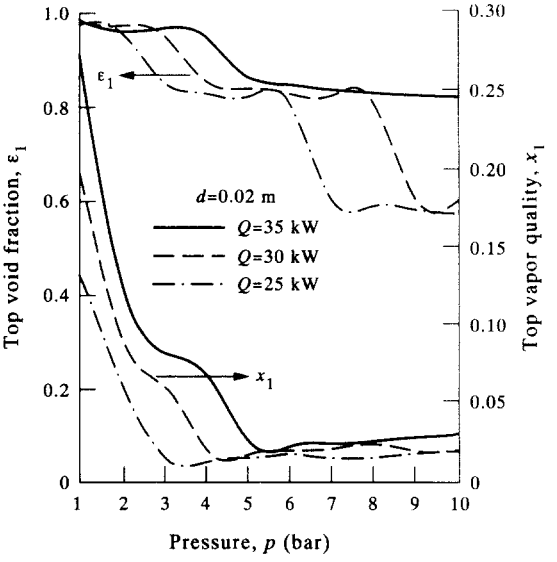

Figure 12. Top void fraction and vapor quality vs loop pressure.

Obviously, higher values of T_0 among the three multiple solutions correspond to lower values of the flow rate.

5.2. *Pressure effects*

When the loop pressure is given, i.e. fixed by a pressurizer, the saturation temperature is determined along with all other fluid properties. The solution for steady-state flow is obtained as explained above. Results for the loop variables as functions of the pressure in the range 1–10 bar are presented for $d = 0.02$ m and three different values of the power input, Q. In cases of multiple solutions only one is taken here, with the highest flow rate, $\dot{m}$.

Figure 11 shows the pressure effect on $\dot{m}$. A local maximum in the curves $\dot{m}(p)$ is observed; this phenomenon, similar to that detected above for $\dot{m}(Q)$, is explained, again, by the behavior of the forces. The friction is reduced when p increases, mainly because the two-phase multiplier decreases

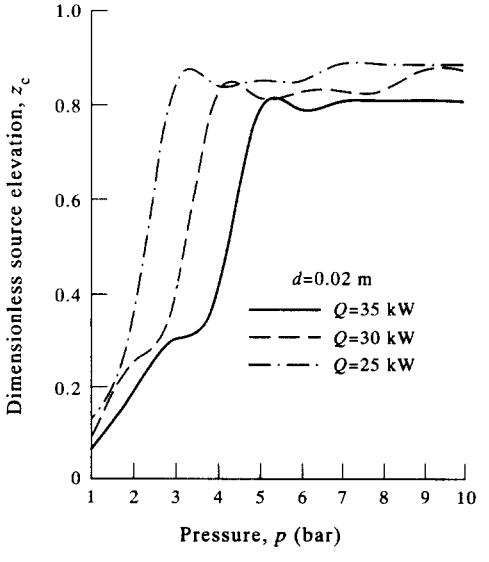

Figure 13. Dimensionless source two-phase elevation vs loop pressure.

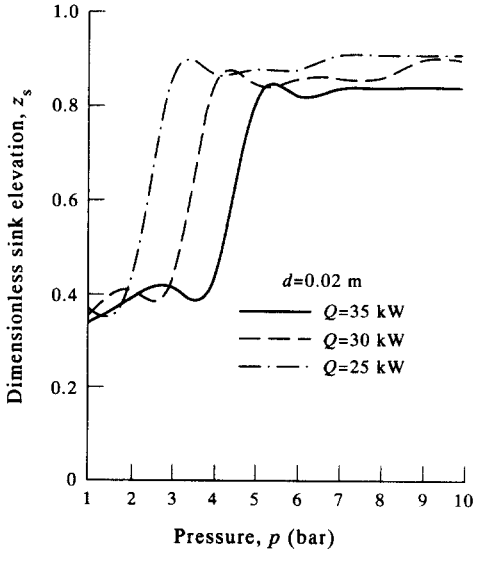

Figure 14. Dimensionless sink two-phase elevation vs loop pressure.

sharply with the quality, which drops steeply when p rises, cf. figure 12. On the other hand, the difference between the two-phase elevations, z_s and z_c, increases at low pressures (figures 13 and 14) causing a strong increase in $\dot{m}(p)$, then becomes almost constant at high pressures, leading to a moderate decrease in $\dot{m}$.

As can be seen from figure 12, the void fraction decreases when p increases, as expected. The flow in the upper portion of the loop is annular at low pressures, small diameters and large powers. As p becomes higher and for larger d and lower Q the flow there does not enter the annular regime; it remains slug, bubbly or single phase (liquid). As mentioned above, the transitions between the flow patterns are associated with discontinuities, as seen in the behavior of ϵ_l (figure 8). The sharp jumps tend to become moderate for higher pressures, because the differences between the properties of the phases are smaller. The two-phase elevations, described in figures 13 and 14, are obviously smaller (larger two-phase portions) at lower p, with $z_c < z_s$, as explained in section 4, Δz is large in this pressure range, yielding the strong buoyancy and rapid increase in the flow rate, discussed above.

The behavior of the bottom temperature, figure 15, may seem somewhat surprising at first glance. The steep increase of T_0 with p at low pressures is explained by the rise in the saturation temperature, T_{sat} enabling the fluid to reach higher temperatures. At some point $T_0(p)$ attains a maximum, earlier at lower Q; this point coincides with that where the top void fraction starts to decrease significantly, see figure 12. The "cooling" in this pressure range is made possible because the flow rate, $\dot{m}$, is near its maximum; the heat transfer coefficient, h_{tp}, is high, thus the heat can be removed to the secondary side in a shorter distance. As p is increased further, $\dot{m}$ decreases (as shown above), and the temperature rises again.

When the thermosyphon system is completely closed (without a pressurizer), the steady state is determined by the specified inventory (total mass), M. The solution is then performed by the computer program with the outermost iteration procedure: guessing p (and reading all the properties from a subroutine), running the inner program to find the solution for this pressure, then calculating M and comparing with the given value, until convergence is achieved. The results are shown in figure 16, giving $p(M)$ for several Q values and $d = 0.02$ m. This figure (or similar ones for other values of Q and d) can be used to obtain the pressure, p, cf. the inventory, M, is known. Then the steady-state variables ($\dot{m}, \epsilon_l, x_l$ etc.) can be found from the figures presented earlier. Complete agreement of the steady-state results was obtained by running the program in the two modes (given p and given M).

Figure 16 shows, as expected that for a given inventory the pressure increases with the power. This can be explained on the basis of the rise of T_{sat} with p. Another interesting phenomenon observed from the figure is the plateau reached for $M(p)$ at high pressures. This follows from the

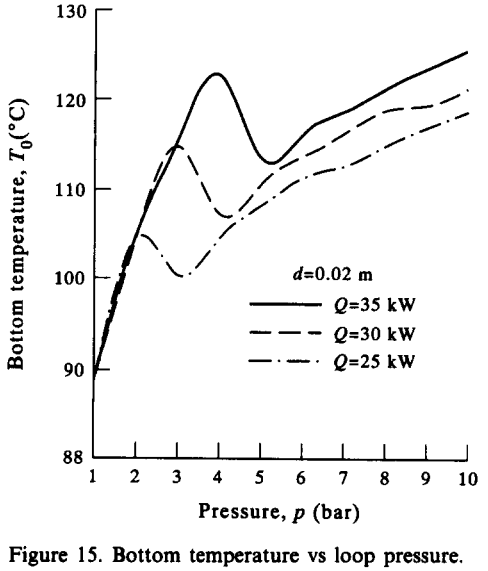

Figure 15. Bottom temperature vs loop pressure.

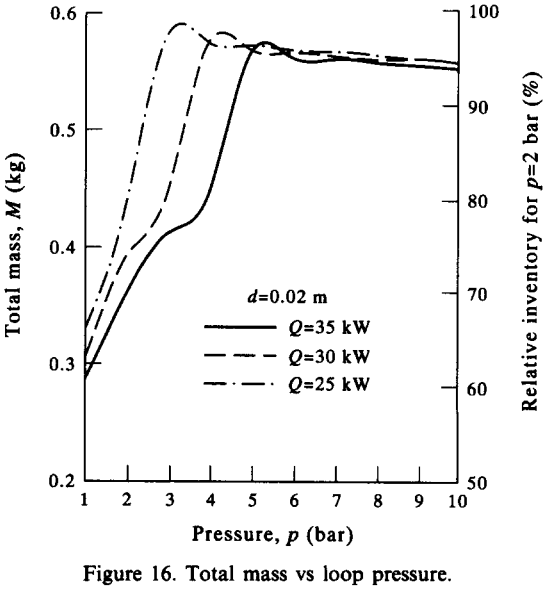

Figure 16. Total mass vs loop pressure.

behavior of the two-phase elevations (figures 13 and 14); z_c and z_s increase with p until a certain value, where boiling in the heat source starts only near the top. Then most of the loop is single phase and the effect of the narrow two-phase portion on the total mass becomes weak.

5.3. Sensitivity to the choice of the flow regimes map

The reader is reminded that the theoretical method and numerical procedure developed in this work are general and can be used to obtain steady-state solutions with any one-dimensional two-phase flow model. Here the drift-flux model was employed to demonstrate application of the method, with the flow regimes map of Kaizerman *et al.* (1983) and heat transfer and friction correlations as described in section 2. The flow regimes map includes transitions from bubbly to slug flow, and slug to annular patterns at certain values of the void fraction. These, chosen "nominally" as $\epsilon_{bs} = 0.25$ and $\epsilon_{sa} = 0.65$, are somewhat arbitrary; in reality the transitions would occur over a finite range of the parameters which also depend on various perturbations.

As an example to illustrate the sensitivity of the results to the choice of the flow regimes map, figure 8 illustrates the behavior of the void fraction distribution in the heat source for three different values of ϵ_{sa} (the other parameters are kept at their nominal values). It is seen that z_c decreases and ϵ_1 increases when ϵ_{sa} is larger. This is explained as follows: when the transition to annular flow is delayed, the values obtained for the void fraction immediately after the switch are larger, because of the behavior of the correlations for C_0 and U_{Gu}. The resulting rise in ϵ_1 (at the top, $z = 1$) causes an increase in the distance needed for condensation ($1-z_s$) and a reduction in the sink two-phase elevation. The buoyancy force becomes smaller, also the flow rate and therefore z_c reduces too.

Figures 17 and 18 show the sensitivity of the solution for $\dot{m}(Q)$ to the choice of the flow regimes map: the values of the void fractions of the transition between slug and annular flow (ϵ_{sa}) in figure 17 and that between bubbly and slug flow (ϵ_{bs}) in figure 18. As ϵ_{sa} is increased, the maximum flow rates become smaller and shift to the left, i.e. at lower values of the input power (figure 17). As mentioned above, when ϵ_{sa} is raised the buoyancy force decreases, and consequently the values of z_c and z_s also become smaller. Thus, x_c and x_s increase, leading to a larger value of the two-phase multiplier Φ^2, indicating augmented friction. The combination of the two effects—lower buoyancy and higher friction—evidently yields reduced velocity and flow rate. On the other hand, when ϵ_{sa} is maintained constant and ϵ_{bs} is increased, only a slight decrease in the maximum $\dot{m}$ is caused (figure 18). The reason for this behavior is that the void at the loop top is not very sensitive to the value of ϵ_{bs}, determining the transition between bubbly and slug flow (which takes place at a relatively lower elevation). Therefore, z_c, z_s and x_c, x_s are not greatly affected and only small changes are felt by the buoyancy and friction forces.

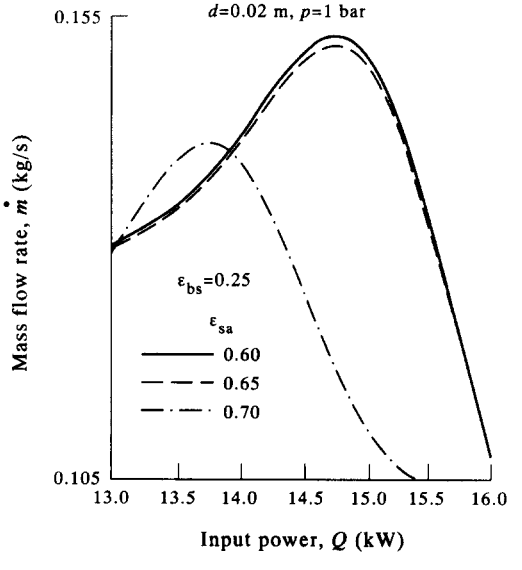

Figure 17. Mass flow rate vs input power; sensitivity to the choice of ϵ_{sa} in the flow regimes map.

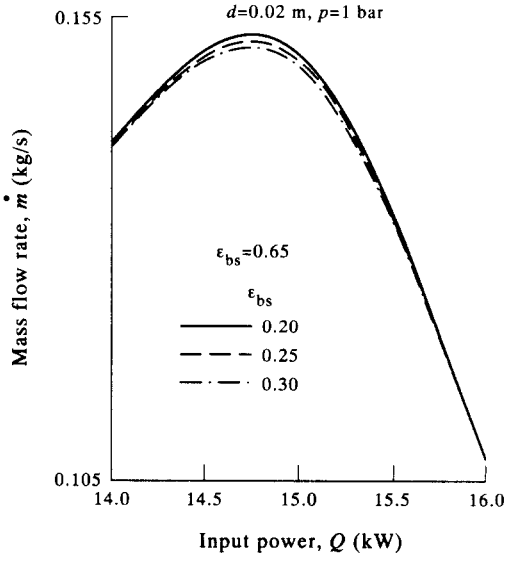

Figure 18. Mass flow rate vs input power; sensitivity to selection of ϵ_{bs} in the flow regimes map.

Table 2 includes results for the loop variables (with $d = 0.02$ m and $p = 2$ bar), as functions of the input power for various choices of the transition values of ϵ_{bs} and ϵ_{sa} in the flow regimes map. The table shows the sensitivity of the multiple steady solutions to the choice of the map. As can be seen from table 2 the value of ϵ_{bs} has a weak effect on the results, while that of ϵ_{sa} affects the solution quite significantly. For example, the maximum flow rate, $\dot{m}$, is lower for larger ϵ_{sa} (0.70), and occurs at a smaller power. The reason for this is probably due to the reduced buoyancy when the transition to annular flow, with more void, is delayed. Similar results were obtained by Knaani & Zvirin (1990) for atmospheric pressure. It is also interesting to note that, for this higher value of ϵ_{sa}, the range of multiple solutions shrinks (a single one is found for $Q = 23$ kW). Obviously,

Table 2. Sensitivity of the multiple steady-state solutions for the mass flow rate, $\dot{m}$, bottom temperature, T_0, top void fraction and vapor quality, ϵ_1 and x_1, and dimensionless two-phase source and sink elevations, z_c and z_s, to the choice of the two-phase flow regimes map ($d = 0.02$ m, $p = 2$ bar)

	ϵ_{bs}:0.25	0.25		0.20	0.30	0.25	0.25		0.20	0.30
Q(kW)	ϵ_{sa}:0.65	0.60	0.70	0.65		0.65	0.60	0.70	0.65	
			$\dot{m}$ (kg/s)					T_0 (°C)		
14.00	0.0943	0.0947	0.0950	0.0945	0.0941	88.9	88.7	88.5	88.8	89.0
16.00	0.1101	0.1106	0.1107	0.1104	0.1099	89.9	89.7	89.7	89.8	90.0
18.00	0.1260	0.1265	0.1251	0.1262	0.1257	91.0	90.8	91.4	90.9	91.1
20.00	0.1417	0.1422	0.1405	0.1419	0.1413	92.1	91.9	92.6	92.0	92.2
22.00	0.1341	0.1351	0.1326	0.1341	0.1316	104.2	104.2	104.2	104.2	104.2
22.00	0.1414	0.1410	0.1428	0.1404	0.1414	101.7	102.1	100.7	102.6	101.7
22.00	0.1565	0.1570	0.1544	0.1565	0.1559	93.6	93.3	94.4	93.5	93.8
23.00	0.1136	0.1340	0.1318	0.1336	0.1310	104.4	104.4	104.3	104.4	104.3
23.00	0.1539	0.1531		0.1526	0.1547	99.0	99.5		99.7	98.5
23.00	0.1622	0.1635		0.1630	0.1617	94.9	94.4		94.6	95.1
24.00	0.1318	0.1328	0.1307	0.1318	0.1318	104.5	104.5	104.5	104.5	104.5
26.00	0.1274	0.1280	0.1263	0.1274	0.1274	104.8	104.8	104.8	104.8	104.8
28.00	0.1224	0.1227	0.1214	0.1224	0.1224	105.0	105.0	105.0	105.0	105.0
30.00	0.1165	0.1168	0.1158	0.1165	0.1165	105.1	105.1	105.1	105.1	105.1
			ϵ_1					x_1		
14.00	0.8195	0.8051	0.6509	0.8130	0.8273	0.0071	0.0064	0.0060	0.0068	0.0075
16.00	0.8288	0.8158	0.6748	0.8226	0.8340	0.0077	0.0070	0.0068	0.0073	0.0080
18.00	0.8411	0.8315	0.8558	0.8369	0.8462	0.0086	0.0080	0.0098	0.0083	0.0090
20.00	0.8567	0.8500	0.8706	0.8531	0.8616	0.0100	0.0094	0.0114	0.0097	0.0105
22.00	0.9587	0.9583	0.9592	0.9587	0.9596	0.0437	0.0431	0.0444	0.0437	0.0450
22.00	0.9470	0.9481	0.9434	0.9495	0.9470	0.0351	0.0360	0.0325	0.0372	0.0351
22.00	0.8787	0.8739	0.8943	0.8781	0.8832	0.0126	0.0119	0.0150	0.0125	0.0132
23.00	0.9612	0.9610	0.9617	0.9612	0.9620	0.0477	0.0475	0.0487	0.0477	0.0492
23.00	0.9338	0.9363		0.9376	0.9312	0.0270	0.0283		0.0290	0.0258
23.00	0.8980	0.8893		0.8929	0.9010	0.0158	0.0142		0.0148	0.0163
24.00	0.9636	0.9633	0.9639	0.9636	0.9636	0.0525	0.0519	0.0532	0.0525	0.0252
26.00	0.9677	0.9675	0.9680	0.9677	0.9677	0.0630	0.0625	0.0638	0.0630	0.0630
28.00	0.9709	0.9709	0.9712	0.9709	0.9709	0.0746	0.0743	0.0754	0.0746	0.0746
30.00	0.9739	0.9738	0.9740	0.9739	0.9739	0.0879	0.0876	0.0885	0.0879	0.0879
			z_c					z_s		
14.00	0.8949	0.9049	0.9108	0.8996	0.8889	0.9128	0.9213	0.9263	0.9168	0.9075
16.00	0.8833	0.8937	0.8959	0.8884	0.8786	0.9021	0.9112	0.9131	0.9066	0.8981
18.00	0.8673	0.8768	0.8503	0.8716	0.8618	0.8876	0.8960	0.8725	0.8914	0.8827
20.00	0.8443	0.8528	0.8236	0.8489	0.8374	0.8666	0.8742	0.8479	0.8708	0.8604
22.00	0.4141	0.4169	0.4100	0.4141	0.4072	0.4489	0.4493	0.4484	0.4489	0.4481
22.00	0.5030	0.4916	0.5361	0.4776	0.5030	0.5310	0.5190	0.5656	0.5043	0.5310
22.00	0.8035	0.8125	0.7688	0.8046	0.7945	0.8289	0.8372	0.7966	0.8300	0.8207
23.00	0.3900	0.3909	0.3852	0.3900	0.3833	0.4428	0.4429	0.4422	0.4428	0.4420
23.00	0.6024	0.5853		0.5762	0.6187	0.6334	0.6160		0.6066	0.6499
23.00	0.7555	0.7779		0.7692	0.7470	0.7838	0.8049		0.7967	0.7757
24.00	0.3651	0.3677	0.3624	0.3651	0.3651	0.4368	0.4371	0.4365	0.4368	0.4368
26.00	0.3204	0.3219	0.3180	0.3204	0.3204	0.4262	0.4263	0.4259	0.4262	0.4262
28.00	0.2823	0.2830	0.2802	0.2823	0.2823	0.4169	0.4170	0.4167	0.4169	0.4169
30.00	0.2485	0.2491	0.2473	0.2485	0.2485	0.4087	0.4087	0.4086	0.4087	0.4087

the transition values ϵ_{bs} and ϵ_{sa} affect the void distribution as seen in figure 6, but for higher powers the differences between the results for various ϵ_{bs} and ϵ_{sa} become smaller (table 2). This follows from the fact that annular flow then prevails in large portions of the loop. Both the buoyancy and friction forces are dominated by the high values of the void and quality in these areas.

It is emphasized that the choice of the limiting values of ϵ_{bs} and ϵ_{sa} in the flow regime map is rather arbitrary. As mentioned above, in reality the transitions between regimes occur over some ranges of the parameters and are triggered by some disturbances. The sensitivity analysis presented here can be considered as an initial attempt to explain and study the related phenomena.

5.4. Comparison with data

Two main results of the present analysis for two-phase natural circulation, discussed in section 5.1, are the bifurcation (multiple steady solutions) and the local maximum in the curves of the flow rate, $\dot{m}$, as a function of the input power, Q. As mentioned above, these phenomena have been observed experimentally and found theoretically not only in such systems but also in single-phase thermosyphons and in other two-phase flows.

Here another important aspect is presented and discussed, namely the behavior of the flow rate, $\dot{m}$, as a function of the loop inventory, MI. It is convenient to represent the steady-state loop characteristics by the curves $\dot{m}(MI)$ (cf. Duffey & Sursock 1987). As indicated by Calastri *et al.* (1990), Juhel *et al.* (1990) and Serre *et al.* (1990), these curves can also be used for scaling purposes. This is quite important in designing and analyzing experiments with scaled models of large loops (cf. Ishii *et al.* 1986; Zvirin & Sursock 1987).

Figure 19 includes curves of the mass flow rate vs the loop inventory for three different values of the input power. When the inventory decreases from 100% (single phase), $\dot{m}$ rises to a maximum and then decreases. This is expected, because when MI is decreased from "water solid" and the loop is more voided, the buoyancy driving force becomes stronger, due to the larger density differences. At high voids (lower inventories) the friction losses counterbalance the buoyancy, increasing more rapidly and reducing the flow rate. When the loop inventory is small, $\dot{m}$ decreases below the single-phase value. These results of the present method, shown in figure 19, agree with the behavior of prototypes and models of two-phase natural circulation loops, as illustrated in the data presented by Duffey & Sursock (1987), Juhel *et al.* (1990), Serre *et al.* (1990) and Calastri *et al.* (1990). There are some differences between the behavior of the loop treated here and the loops

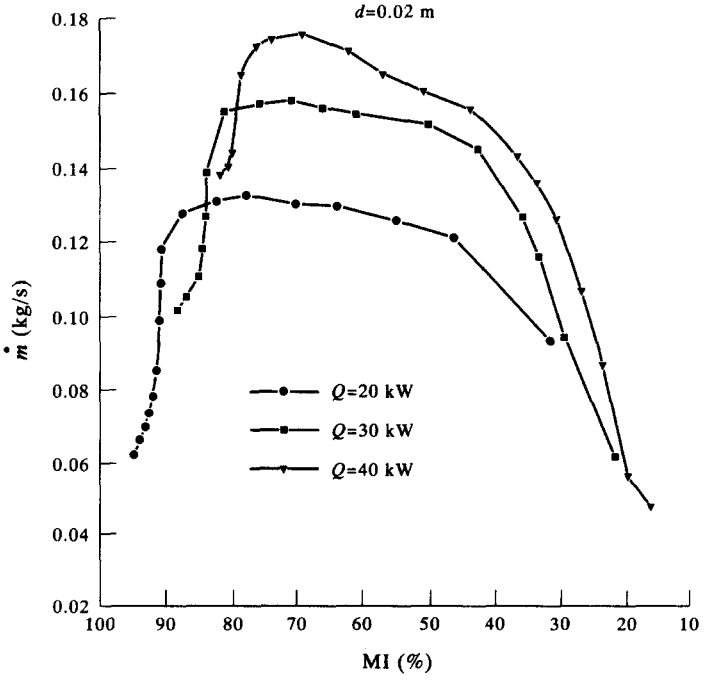

Figure 19. Mass flow rate vs loop inventory.

considered in these references. Firstly, when MI is decreased from 100% the rise of $\dot{m}$ is almost immediate here, while in the data it is moderate (plateau-like), with a sharp increase in $MI = 90$ to 95%. This is explained by the different geometries: here, with the simplified loop consisting of two vertical pipes, small voids lead to large density differences and strong driving buoyancy forces; in the experimental loops, with geometries of nuclear reactor systems, the bulk of the fluid is contained in the reactor vessel, so larger voids are needed to create significant buoyancy forces for driving relatively larger liquid masses. The differences in the geometries of the present simplified thermosyphon and the loops considered in the above references also lead to the different location of the peaks in the curves $\dot{m}(MI)$. They are at smaller values here ($MI = 70$–75%) than in the experimental systems, mostly in the range 75–82%. Here the effect of the friction is sensed more rapidly, because of the larger ratio of tube surface to loop volume. However, in the neighborhood of the peak, the curves here are more flattened, due to the stronger buoyancy influence mentioned above. Finally, the references cited here show some numerical results obtained from computer codes used to simulate reactor cooling loops. The general agreement between these and the data are also quite good, but many differences still appear.

6. SUMMARY

A general and consistent theoretical method was developed to study the steady-state flow and heat transfer in two-phase thermosyphons. Numerical calculations were carried out, using the one-dimensional drift-flux model and flow regimes map. Results have been presented to investigate the effect of the loop geometry, the pressure and the input power on the loop variables, e.g. flow rate, void quality and temperature distributions and two-phase elevations.

The loop exhibits bifurcation characteristics, i.e. there exist multiple steady-state solutions in a certain range of the parameters. This phenomenon has obvious impacts on the operation of practical loops such as energy conversion systems, and in particular emergency core cooling of nuclear reactors. Several other important and interesting results have been observed, including the appearance of a local maximum of the flow rate curves as functions of the input power and of the pressure. A comparison with available data has shown that these results follow the behavior and trends of experimental loops, and the general appearance of code predictions. The sensitivity of the results to the choice of the flow regimes map was also investigated. The results indicate the applicability of the method, which can be used in the design of efficient stable loops and prediction of their performance.

As explained above, a theoretical–numerical analysis of a thermosyphon, taking into account the various two-phase flow regimes and patterns, is quite complicated. Therefore, treatment of a simple geometry loop (figure 1) was chosen as the first stage in developing the method. Following the demonstration that it can describe the loop behavior, it is planned, in the next stage of the research program, to investigate transient flows in systems representing more realistic loops, and also to study their stability.

Acknowledgements—This work was carried out at the Technion (IIT) as partial fulfillment of the requirements for the M.Sc. in Mechanical Engineering of A. Knaani. The work was partially supported by the Israel-Mexico Energy Research Fund, to whom the authors are grateful.

REFERENCES

ARDRON, K. H. & KRISHNAN, V. S. 1984 Stability of a two phase natural circulation loop with figure-of-eight symmetry. In *Multiphase and Heat Transfer III*, Part A (Edited by VEZIROGLU, T. N. & BERGLES, A. E.), pp. 849–870. Elsevier Science, Amsterdam.

BARNEA, D. 1987 A unified model for predicting flow pattern transitions for the whole range of pipe inclinations. *Int. J. Multiphase Flow* **13**, 1–12.

BOURÉ, J. & MIKAILA, A. 1967 The oscillatory behavior of heated channels. In *Proc. Symp. on Two*-phase *Flow Dynamics*, Eindhoven, The Netherlands, Vol. 1, pp. 695–720.

CALASTRI, A., D'AURIA, F., GALASSI, G. M. & VIGNI, P. 1990 Scaling of natural circulation in PWR systems. In *Proc. Eurotherm Semin. No. 16: Natural Circulation in Industrial Applications*, Pisa, Italy, pp. 143–157.

CHATO, J. C. 1963 Natural circulation flows in parallel channels. *J. Heat Transfer* **85,** 339–345.

CHEXAL, B. & LELLOUCHE, G. 1985/1986 A full range drift flux correlation for vertical flows. Reports EPRI NP-3989-SR/Revision 1.

CHISHOLM, D. 1967 A theoretical basis for the Lockhart–Martinelli correlation for two phase flow. *Int. J. Heat Mass Transfer* **10,** 1767–1778.

COLLIER, J. G. 1972 *Convective Boiling and Condensation.* McGraw-Hill, London.

CUNDY, V. A. & HA, L. 1982 The characterization of a gravity assisted heat pipe with internal two phase parallel flow throughflow. In *Thermal Sciences 16,* Vol. 2 (Edited by VEZIROGLU, T. N.), pp. 599–612. Hemisphere, Washington, DC.

DUFFEY, R. B. & SURSOCK, J. P. 1987 Natural circulation phenomena relevant to small breaks and transients. *Nucl. Sci. Engng* **102,** 115–128.

GREIF, R. 1988 Natural circulation loops. *J. Heat Transfer* **110,** 1243–1258.

GROSSMAN, G., GOMMED, K. & GADOTH, D. 1987 A computer program for simulation of absorption systems in flexible and modular form. *ASHRAE Trans.* **93,** 2389–2428.

HART, J. E. 1984 A new analysis of a closed loop thermosyphon. *Int. J. Heat Mass Transfer* **27,** 125–136.

HETSRONI, G. 1982 *Handbook of Multiphase Systems.* McGraw-Hill, London.

ISHII, M. & KATAOKA, I. 1983 Similarity analysis and scaling criteria for LWRs under single-phase and two-phase natural circulation. Argonne National Laboratory Reports NUREG/CR-3267 & ANL-82-32.

ISHII, M. & ZUBER, N. 1970 Thermally induced flow instabilities in two-phase mixtures. In *Proc. 4th Int. Heat Transfer Conf.*, Paris-Versailles, Vol. 5, Paper B5.11.

ISHII, M., KOCAMUSTAFAOGULLARI, G. & KATAOKA, I. 1986 Pressure and fluid to fluid scaling laws for two-phase flow loop. In *Proc. 8th Int. Heat Transfer Conf.*, San Francisco, CA, Vol. 5, pp. 2259–2264.

JEUCK, P. III, LENNERT, L. & KIANG, R. L. 1981 Single-phase circulation experiments on small-break accident heat removal. Report EPRI NP-2006.

JUHEL, D., BAZIN, P., BRIDAY, G., DUMONT, D. & NOEL, B. 1990 Bethsy natural circulation program and present results. In *Proc. Eurotherm Semin. No. 16: Natural Circulation in Industrial Applications*, Pisa, Italy, pp. 95–102.

KAIZERMAN, S., WACHOLDER, E. & ELIAS, E. 1982 Characteristics analysis of one-dimensional two-phase flow using the drift-flux model. Report TNED-R/574, Dept of Nucl. Engng, Technion, IIT, Haifa, Israel.

KAIZERMAN, S., WACHOLDER, E. & ELIAS, E. 1983 A drift-flux model flow regime map of two phase flows for thermal hydraulic calculation. *Nucl. Sci. Engng* **84,** 166–168.

KIANG, R. L. 1985 Scaling criteria for nuclear reactor thermal hydraulics. *Nucl. Sci. Engng* **89,** 207–216.

KIANG, R. L. & MARKS, J. S. 1981 Two-phase natural circulation experiments on small break accident heat removal. Report EPRI NP-2007.

KNAANI, A. 1990 Investigation of a two phase natural circulation loop. M.Sc. Thesis, Faculty of Mechanical Engng, Technion, IIT, Haifa, Israel.

KNAANI, A. & ZVIRIN, Y. 1990 Investigation of a two phase natural circulation loop. In *Proc. 9th Int. Heat Transfer Conf.*, Jerusalem, Israel, Vol. 3, pp. 395–400.

LOOMIS, G. G. & SODA, K. 1982 Results of the semiscale Mod-2A natural circulation experiments. NRC, INEL Report NUREG/CR-2335.

MCKEE, H. R. 1970 Thermosyphon reboilers—a review. *Ind. Engng Chem.* **62,** 76–82.

MERTOL, A., GREIF, R. & ZVIRIN, Y. 1981 The transient, steady state and stability behavior of a natural convection loop with a throughflow. *Int. J. Heat Mass Transfer* **24,** 621–633.

NGUYEN-CHI, H. & BANERJEE, S. 1984 Experimental data report on condensation in a single inverted U-tube. Report EPRI NP-3471.

PIRET, E. L. & ISBIN, H. S. 1954 Natural circulation evaporation. *Chem. Engng Prog.* **50,** 305–311.

RAMOS, E., SEN, M. & TREVIÑO, C. 1985 A steady-state analysis for variable area one- and two-phase thermosyphon loops. *Int. J. Heat Mass Transfer* **28,** 1711–1719.

REED, J. G. & TIEN, C. L. 1987 Modeling of a two-phase closed thermosyphon. *J. Heat Transfer* **109,** 722–730.

RUBENFELD, L. A. & SIEGMANN, W. L. 1977 Nonlinear dynamic theory for a double diffusive convective model. *SIAM Jl Appl. Math.* **32,** 871–894.

SEN, M. & TREVIÑO, C. 1983 One dimensional thermosyphon analysis. *Latin Am. J. Heat Mass Transfer* **7,** 135–150.

SERRE, F., YONOMOTO, T., KUKITA, Y. & TASAKA, K. 1990 CATHARE analysis of natural circulation under normal and degraded secondary cooling conditions in LSTF runs ST-NC-06 and ST-NC-07. In *Proc. Eurotherm Semin. No. 16: Natural Circulation in Industrial Applications*, Pisa, Italy, pp. 103–110.

SHIMECK, D. J. & JOHNSEN, G. W. 1984 Natural circulation cooling in a PWR geometry under accident induced conditions. *Nucl. Sci. Engng* **88,** 321–330.

WISSLER, E. H., ISBIN, H. S. & AMUNDSON, N. R. 1956 Oscillatory behavior of a two-phase natural circulation loop. *AIChE Jl* **2,** 157–162.

ZVIRIN, Y. 1981 A review of natural circulation loops in pressurized water reactors and other systems. *Nucl. Engng Des.* **67,** 203–225.

ZVIRIN, Y. 1985 The instability associated with the onset of motion in a thermosyphon. *Int. J. Heat Mass Transfer* **28,** 2105–2111.

ZVIRIN, Y. 1986 The onset of flows and instabilities in a thermosyphon with parallel loops. *Nucl. Engng Des.* **92,** 217–226.

ZVIRIN, Y. 1987 Instabilities in a double-diffusive thermosyphon. *Int. J. Heat Mass Transfer* **30,** 1319–1329.

ZVIRIN, Y. 1991 Transient and stability phenomena in a double diffusive natural circulation loop. *Int. J. Heat Mass Transfer* **34,** 543–558.

ZVIRIN, Y. & SURSOCK, J. P. 1987 Scaling of two-phase natural circulation experiments. In *ANS Proc. U.S. Natn. Heat Transfer Conf.*, Pittsburgh, PA, pp. 31–39.